UC San Diego
UC San Diego Previously Published Works

Title

A probabilistic approach for the optimisation of ultrasonic array inspection techniques

Permalink

https://escholarship.org/uc/item/2fd099jh

Authors

Humeida, Yousif
Wilcox, Paul D
Todd, Michael D
et al.

Publication Date

2014-12-01

DOI

10.1016/j.ndteint.2014.07.007

Peer reviewed

A probabilistic approach for the optimisation of ultrasonic array inspection techniques

Yousif Humeida [a,*], Paul D. Wilcox [a], Michael D. Todd [b], and Bruce W. Drinkwater [a]

[a] Department of Mechanical Engineering, University Walk, University of Bristol, Bristol BS8 1TR, UK
[b] University of California, San Diego, 9500 Gilman Dr. 0085, La Jolla, CA 92093-0085, USA

[*] Corresponding author. E-mail address: y.humeida@bristol.ac.uk (Y. Humeida)

Abstract

Ultrasonic arrays are now used routinely for the inspection of engineering structures in order to maintain their integrity and assess their performance. Such inspections are usually optimised manually using empirical measurements and parametric studies which are laborious, time-consuming, and may not result in an optimal approach. In this paper, a general framework for the optimisation of ultrasonic array inspection techniques in NDE is presented. Defect detection rate is set as the main inspection objective and used to assess the performance of the optimisation framework. Statistical modelling of the inspection is used to form the optimisation problem and incorporate inspection uncertainty such as crack type and location, material properties and geometry, etc. A genetic algorithm is used to solve the global optimisation problem. As a demonstration, the optimisation framework is used with two objective functions based on array signal amplitude and signal-to-noise ratio (SNR). The optimal use of plane B-scan and total focusing method imaging algorithms is also investigated. Performance of the optimisation scheme is explored in simulation and then validated experimentally. It has been found that, for the inspection scenarios considered, TFM provides better detectability in a statistical sense than plane B-scan imaging in inspection scenarios with uncertainty.

1. Introduction

The use of ultrasonic arrays for non-destructive evaluation (NDE) applications has grown rapidly in recent years. Arrays have key advantages over single element transducers in terms of sensitivity and inspection performance. The take-up of array technology has been across a wide range of industrial sectors including power generation, aerospace, oil and gas and automotive. For example, in the power generation industry, Mahaut et al. [1] describe the inspection of welds in thick (30-50 mm) steel plates using a conformable array. They show the use of an array to steer the beam through a range of angles thus ensuring sensitivity to a range of crack angles in geometrically complex components.

Some attempts have been made to optimise ultrasonic array systems for medical applications where it is reasonable to assume the array elements emit into an infinite fluid filled half-space. For example, Matte et al. [2] and Ergun [3] investigate the

optimal array geometry and frequency for harmonic imaging and therapeutic ultrasound respectively. However, both authors focus on a small number of parameters, and hence can plot optima on 2D and 3D graphs. A number of authors have considered the problem of optimal placement of array elements (sources) for both medical and general purpose imaging. Nikolov and Behar [4] use a simulated annealing algorithm to find the element weighting functions that achieve the optimal image contrast (i.e. signal to imaging artefact ratio) and lateral resolution. Martinez-Graullera et al. [5] and Raju et al [6] investigate the optimisation of imaging performance metrics using sparse arrays. They both use sparse patterns described by a small number of parameters to simplify the optimisation problem and then perform the optimisation by completely exploring the resulting parameter space.

Forward modelling is increasingly used to inform and improve array inspections for NDE. For example Mahaut et al. [7] and Zhang et al. [8] use hybrid approaches in which the wave propagation through the body of the component is modelled as a ray (or pencil beam) and the scattering from a defect is modelled using analytical or finite element approaches. To date these forward models are used pragmatically to inform the array inspection process, rather than to fully explore the relevant parameter space to find optimal configurations. The one recent exception being the work done by Puel et al. [9] who have demonstrated array optimisation of a simple amplitude based cost function using a commercial ultrasonic modelling package CIVA (which is developed by the CEA, French Atomic Energy Commission) as their forward model. One of the problems in the optimisation approach adopted in their work is that deterministic forward models have been used to optimise the array inspection for the imaging of a particular defect at a particular location within the considered specimen. In most inspection scenarios, certain levels of uncertainty occur related to the type, size, and location of the defects to be detected or the properties and geometry of the material that need to be inspected.

Here we present a general framework for the optimisation of ultrasonic array inspection techniques in NDE. Both forward deterministic and statistical modelling of the inspection are used to formulate the optimisation problem and incorporate inspection uncertainty information. The array produces an image of the interior of the test structure and these images can be used for both detection and characterisation. This work follows the approach presented by Flynn and Todd [10] who present a theoretical framework based on detection theory for optimal sensor placement in structural health monitoring (SHM) applications using ultrasonic guided waves. Here we explore a simple inspection set-up in which defect detection has been defined as the main inspection objective and use this to assess the performance of the optimisation framework. Experimental measurements are carried out for benchmarking and validation.

2. Optimisation framework

In this study, the defect detection problem is expressed in the form of an optimisation problem. Optimisation problems can be described in a general form as follows: Given a set of variables X (*decision variables*) and a set of functions $Y: X \rightarrow \mathbb{R}$ (the *objective functions*), the aim is to find $x^* \in X$ such that for all $x \in X$, there holds $Y(x) < Y(x^*)$.

In the current ultrasonic array inspection problem, the array location, propagation mode(s), coupling method, array size, number of elements, etc. are considered as the *decision variables*. For a deterministically defined inspection problem, the imaging signal amplitude, SNR, etc. can be considered as objective functions whereas for a stochastic problem, a statistical parameter such as the mean, median, minimum, or cumulative probability above a threshold for the signal amplitude or the SNR can be considered as an objective function. These objective functions will be chosen depending on the aim of the inspection (i.e. detection, characterisation, or both), and they will depend on the component geometry, material properties, defect type, location, and orientation. Some of these parameters might be precisely known and well-defined while some others might be uncertain.

Here we address the stochastic problem by using deterministic forward models to calculate realisations of these objective functions, and a Monte Carlo approach to heuristically simulate uncertainty in the inspection. In many cases, these objective functions are expected to be fairly challenging to maximise and contain multiple maxima. Therefore, global optimisation algorithms, such as the genetic algorithm (GA), simulated annealing (SA), or Monte Carlo Markov Chains (MCMC) can be used to solve these optimisation problems.

Fig. 1 shows a flowchart of the proposed optimisation framework. The following sections will describe the main components of this optimisation framework which will then be used to optimise the inspection in two specific examples. The optimisation results will also be validated experimentally.

2.1. Forward model

In this optimisation framework, a frequency-domain far-field hybrid modelling approach is used to simulate the forward problem. In this hybrid model a ray-based model is used to simulate the propagation of ultrasonic waves through the body of the structure while a scattering coefficient matrix is used to model the response of the defect. The ray model analytically incorporates the effects of beam divergence, phase delays, refraction, and mode conversion at interfaces. The scattering coefficient of a defect describes its far-field ultrasonic response as a function of the angle of incidence and scattering. These scattering coefficients can be calculated using analytical or finite element (FE) methods [7, 8].

As shown in Fig. 2, a signal emitted from the transmitter, propagates through the material, and scatters from the defect back to the receiver. A generalised formula for the received signal strength can be given as follows [11]:

$$H(\boldsymbol{e_t}, \boldsymbol{e_r}, \boldsymbol{e'}, \omega) = \qquad\qquad 1$$
$$[A(\omega)]^2 D(\boldsymbol{e_t}, \boldsymbol{e'}, \omega) E(\boldsymbol{e_t}, \boldsymbol{e'}, \omega) D(\boldsymbol{e_r}, \boldsymbol{e'}, \omega) E(\boldsymbol{e_r}, \boldsymbol{e'}, \omega) S(\boldsymbol{e_t}, \boldsymbol{e_r}, \boldsymbol{e'}, \omega),$$

where $H(\boldsymbol{e_t}, \boldsymbol{e_r}, \boldsymbol{e'}, \omega)$ is the signal transmitted from an array element at a position $\boldsymbol{e_t}$, scattered by a scatterer at $\boldsymbol{e'}$, and received by an element at $\boldsymbol{e_r}$, $A(\omega)$ is the frequency response of an array element, $D(\boldsymbol{e_m}, \boldsymbol{e'}, \omega)$ is the directivity/sensitivity of array element m in the direction of the scatterer at $\boldsymbol{e'}$, $E(\boldsymbol{e_t}, \boldsymbol{e'}, \omega)$ is the system (component) transfer function associated with array element m and the scatterer at $\boldsymbol{e'}$, $S(\boldsymbol{e_t}, \boldsymbol{e_r}, \boldsymbol{e'}, \omega)$ is the defect scattering coefficient matrix, ω is the angular frequency, and the subscripts t and r denote the transmit and the receive ray paths, respectively. Fig. 2 and equation 1 represent a general model for an ultrasonic inspection system which can easily be modified or extended depending on the inspection scenario.

The system transfer function, $E(\boldsymbol{e_t}, \boldsymbol{e'}, \omega)$, depends on the dimensions and properties of the structure. In homogenous media, waves are assumed to propagate in straight lines. At interfaces, Fermat's minimum time principle is used to calculate the direction of propagation and the system transfer function will depend on the transmission and reflection coefficients at these interfaces. It also accounts for the phase delay and amplitude loss through beam divergence and attenuation. The scattering coefficient of the defect, $S(\boldsymbol{e_t}, \boldsymbol{e_r}, \boldsymbol{e'}, \omega)$, depends on its type, size, and orientation. Analytical solutions such as the separation of variables, Kirchhoff, Born approximations, and FE methods may be used to characterise the defects' scattering coefficients. In this study, an analytical solution for planar cracks response to ultrasonic signals derived by Glushkov et al. [12] is used.

2.1.1. Array imaging

For an array, the model described in section 2.1 can be used to calculate signals for all the different combinations of transmit and receive of the array elements. Then, this matrix of data can be used in post-processing to perform different types of imaging algorithm such as plane B-scans, focused B-scans, and the total focusing method (TFM). These can then be utilised to calculate the optimisation objective function [13].

In a plane B-scan, signals from a continuous group of array elements (an aperture) are synthetically pulsed simultaneously into the material and all the signals received at all elements in the aperture are summed to produce the output signal. A plane B-scan image is equivalent to that obtained by using a single transducer with a size equivalent to that of the plane B-scan aperture:

$$I(\boldsymbol{e}, \omega) = \left| \sum H(\boldsymbol{e_t}, \boldsymbol{e_r}, \boldsymbol{e'}, \omega) e^{-j\omega\frac{2\boldsymbol{e}\cdot\hat{\boldsymbol{z}}}{c}} \right| \tag{2}$$

summed for $|\boldsymbol{e_t} - \boldsymbol{e}| \cdot \hat{\boldsymbol{x}} \leq N_A$ and $|\boldsymbol{e_r} - \boldsymbol{e}| \cdot \hat{\boldsymbol{x}} \leq N_A$

where $I(\boldsymbol{e}, \omega)$ is image magnitude at an arbitrary position $\boldsymbol{e}$, $\hat{\boldsymbol{z}}$ is the unit vector in the z direction, c is the speed of sound in the material, and N_A is the array aperture size. $N_A \leq N$, where N is the total size of the array.

In the TFM, the different elements of the aperture are synthetically pulsed at different instances of time (different phases) to enable the array to focus at particular points within the material. Different delays are used to calculate signals at different locations:

$$I(\boldsymbol{e}, \omega) = \left| \sum H(\boldsymbol{e_t}, \boldsymbol{e_r}, \boldsymbol{e'}, \omega) e^{-j\omega\frac{|\boldsymbol{e_t}-\boldsymbol{e}|+|\boldsymbol{e_r}-\boldsymbol{e}|}{c}} \right| \tag{3}$$

for all t and r

2.1.2.   Noise model

There are many sources of noise in ultrasonic signals. Here, electrical noise and structural noise are considered to be the main such sources. However, structural noise (the noise due to the back-scatter from the grains in metals) is what ultimately limits the detectability of defects [14]. Many studies have been dedicated to the analysis of grain noise in materials. For a single transducer measurement and using a single scattering model, it has been found that the root mean square (RMS) noise can be characterised using the acoustic properties of the material, the density of grains per unit volume, and their back-scattered signal amplitude [15, 16]. Similarly when ultrasonic imaging is used, it is found that the RMS noise will depend on the mean ultrasonic back-scatter per unit volume and on the RMS of the transfer function of the imaging algorithm as shown in equation 4 [14]:

$$\sqrt{\langle |n(\boldsymbol{e})|^2 \rangle} = \sigma_n \sqrt{\int |p(\boldsymbol{e}, \boldsymbol{e'})|^2 d\boldsymbol{e'}} \tag{4}$$

where $\sqrt{\langle |n(\boldsymbol{e})|^2 \rangle}$ is the RMS noise value, σ_n is the mean ultrasonic back-scatter per unit volume, and $p(\boldsymbol{e}, \boldsymbol{e'})$ is the point spread function (PSF) of the imaging method at the location $\boldsymbol{e}$ due to point scatterer at $\boldsymbol{e'}$. Fig. 3 shows the magnitude of a TFM PSF for a point reflector at a depth of 20 mm in an aluminium plate using an ultrasonic array with 32 elements, 5 MHz centre frequency, and 0.63 mm element pitch. This PSF is then squared and summed over the whole area of the image to calculate the RMS noise in equation 4.

2.2.Stochastic modelling

In a typical array inspection, some parameters of the solution of equation 1 are expected to be uncertain. Materials might contain defects with different sizes, orientations, and shapes. Furthermore, there might also be some difficulties in determining accurate values for the component dimensions or properties; examples include thin-walled pipes with weld caps and austenitic welds with inhomogeneous anisotropic properties [17]. This uncertainty transforms the deterministic inspection problem into a stochastic one. It is assumed that when this uncertainty is present, it can be characterised statistically using a probability density function (PDF). Here we use a Monte Carlo method to run many realisations of the deterministic forward model to represent the inspection uncertainty. The ultrasonic response is then optimised via recursive calculation of these Monte Carlo realisations using a GA.

2.3.Optimisation algorithm

Global optimisation algorithms are used in this study to solve the optimisation problem as they are known to be efficient in incorporating statistical information and dealing with complicated objective functions that have multiple local minima/maxima. The genetic algorithm (GA) is such a global optimisation technique that mimics biological evolution processes and is used in this particular study. The algorithm starts with a random selection of a population from the decision variable domain (X). The genetic algorithm repeatedly modifies this population. At each step, the algorithm selects a group of individual values from the population (parent) which are evolved through crossover or mutation to produce members of the next generation. This process is repeated for several generations until an optimum solution is reached. See [18] for a fuller description of the GA.

2.4.Defect detection

The primary focus of this paper is the detection of defects (as opposed to, for example, defect location). Therefore, a binary statistical hypothesis test has been adopted. In such system, there are only two possible states: either a defect is not present (this is called the *null hypothesis*, $\mathcal{H}_0$) or a defect is present (this is called the *alternative hypothesis*, $\mathcal{H}_1$). In the absence of a defect, only noise signals will be present, while in the presence of a defect, both noise and defect signals will exist [10, 19].

Let us assume that both defect signals and noise can be presented by realisations of random variables I and n, respectively.

Fig. 4 shows a PDF representation of these two random signals. A decision will be made by setting a threshold (T) as shown in the figure. Whenever a sample (h) is observed, the null hypothesis will be accepted if $h < T$. Otherwise, i.e. when $h > T$, the null hypothesis will be rejected in the favour of the alternative hypothesis.

It is clear that with the above scheme, two types of errors might occur: Type I error (when $\mathcal{H}_1$ is decided but $\mathcal{H}_0$ is true) and Type II error (when $\mathcal{H}_0$ is decide but $\mathcal{H}_1$ is true). Any chosen threshold (T) will always be a trade-off between these two errors. A particular threshold can be chosen to reduce Type I error but as a result Type II error will increase and vice-versa. The overall detection performance can be characterised by plotting receiver operating characteristic (ROC) curves. A receiver operating characteristic (ROC) curve relates the complement of Type II error (the probability of detection, P_D) to Type I error (the probability of false alarm, P_{FA}). Each point in the ROC curve is obtained by choosing a particular threshold (T) and hence by changing the value of this threshold, the ROC curve is obtained.

3. Optimisation demonstration

The optimisation framework described in section 2 has been used to optimise the array measurement of cracks in aluminium plates using a contact array. It is assumed that the aluminium has a density of 2700 kg/m^3 and a longitudinal and a shear wave velocity of 6432 m/s and 3100 m/s, respectively. It has also been assumed that there is a possibility that the aluminium sample will contain a 3 mm crack with a stochastic orientation angle. The PDF of the crack orientation angle is assumed to be a normal distribution function $N(\mu_s, \sigma_s)$, where the mean (μ_s) is always assumed to be 0°. The crack is assumed to be at a depth of 20 mm at all times as shown in Fig. 5.

In this case the optimisation problem has been formulated such that there are some deterministic parameters such as the dimensions and properties of the aluminium sample and the location and size of the crack. The only uncertain parameter in this case is the orientation of the 3 mm crack which, in terms of the forward model, will manifest itself in the crack scattering coefficient.

Only single-frequency calculations have been used in the forward model to reduce the computational time needed to carry out the optimisation process. The simulated frequencies are chosen as the central frequencies of the experimental signals. A 2-D model based on equation 1 has been used to calculate the array signal amplitudes. The only wave mode that has been used for this inspection is the longitudinal mode. The directivity, $D(\boldsymbol{e_m}, \boldsymbol{e'}, \omega)$, of 1-D linear arrays elements is modelled using a 2-D solution in the far field shown in [20]. This solution assumes that array elements behave as a strip source and their response can be derived by integrating the field provided by Miller and Pursey [21] from line sources in the isotropic material of interest.

The system transfer function, $E(\boldsymbol{e_m}, \boldsymbol{e'}, \omega)$, in this case consists of two components: the signal phase shift and the divergence factor. Both of these factors depend on the distance from the transmitting element to the crack and back from the crack to the receiving element. The system function, $E(\boldsymbol{e_m}, \boldsymbol{e'}, \omega)$, is given as follows [13]:

$$E(\boldsymbol{e_m}, \boldsymbol{e'}, \omega) = \frac{e^{-j\omega|\boldsymbol{e_m}-\boldsymbol{e'}|/c}}{\sqrt{|\boldsymbol{e_m} - \boldsymbol{e'}|}} \hspace{4cm} 5$$

where $|\boldsymbol{e_m} - \boldsymbol{e'}|$ is the distance from the array element m to the crack at location $\boldsymbol{e'}$.

An analytical solution [12] is used to calculate the 2-D scattering coefficients, $S(\boldsymbol{e_t}, \boldsymbol{e_r}, \boldsymbol{e'}, \omega)$, for the 3 mm crack, which is used in this example. The response from 50 cracks with normally-distributed random orientation angles (θ_s) was then simulated using the forward model for use in the optimisation scheme.

Following are two demonstration examples in which different objective functions and optimisation variables have been used.

In both examples, different crack orientation standard deviations (σ_s) have been used throughout the simulations (0, 2, 4, 6, 8, 10 and 15°). The case in which the standard deviation is 0° is simply a single crack with an orientation angle of 0°. A GA with a population of 50 and 30 generations has been used to maximise the objective function for all cases.

3.1. Example 1: optimising frequency and aperture size

In the first demonstration example, a linear array with the specifications shown in Table 1 is chosen. In all cases mechanical scanning along the surface of the aluminium plate is simulated to arrive at an optimum inspection location. Fig. 6 (a) shows a schematic diagram that describes this inspection set-up.

The only design specifications that are allowed to vary in this case are the size of the array aperture (N_A) and the operational angular frequency (ω). All other array specifications are fixed as described in Table 1. It can be noted from the table that the array size and the frequency (which are the decision variables) are constrained to the values 0.63 mm to 20.2 mm (i.e. 1 to 32 elements) and 3 to 7 MHz, respectively. A maximum of 32 elements was considered in the calculations to limit the computational time which increases as the number of elements increase. The range of frequencies chosen was governed by the bandwidth of the wideband ultrasonic array that is later used for experimental validation.

The objective function in this example has been chosen to be the array signal amplitude of the worst-case-scenario (i.e. the response from the crack that produces the minimum signal amplitude, $I(\boldsymbol{e'}, N_A, \omega)_{min}$). Mathematically, the optimisation problem can be expressed using this objective function as follows:

$$\max I(\boldsymbol{e'}, N_A, \omega)_{min} \hspace{4cm} 6$$

where the values of N_A and ω are constraints by the values shown in Table 1.

3.1.1. Optimisation results

Results for the optimum array aperture (N_A) and angular frequency (ω) using the plane B-scan and the TFM are shown in Table 2.

If we take the case when the standard deviation is 4°, as an example Fig. 7 shows how the optimisation algorithm works and how the results evolve through the different generations to arrive at an optimum value when either plane B-scans or the TFM are used.

The optimal designs shown in Table 2 have been used to simulate images of individual cracks to compare the performance of these optima. Signals with a bandwidth of 2 MHz around the central operating frequency were used. Two cracks (at 0 and 45°) are shown and Fig. 8 compares the plane B-scans for these cracks generated using two optimal arrays, i.e. (7 MHz, 7.6 mm) and (3 MHz, 18.3 mm). It can be noted that while the (7MHz, 7.6 mm) array gives the maximum image amplitude for the 0° crack, the (3MHz, 18.3 mm) array performs better for detecting the 45° crack. Similarly, TFM images for the 0 and 45° cracks have been generated using the 7MHz, 20.2 mm array.

3.1.2. Experimental validation

Due to the difficulty of manufacturing enough aluminium plates with cracks at different orientation angles to resemble the different PDFs used in the simulations, 4 aluminium plates, see Fig. 5, with 3 mm slots at angles of 0, 15, 30, and 45° have been used to validate the simulation results presented in the previous section. Experiments have been carried out using a wideband 5 MHz linear array with 64 elements (manufactured by Imasonic, Besancon, France) to find the optimum operation angular frequency (ω) and size (N_A) to maximise the signal amplitude from the 4 different slots. The array has the same specifications as shown in Table 1. As mentioned earlier, frequency calculations have been limited to the range from 3 to 7 MHz which is the usable bandwidth of the array. A Gaussian filter with a bandwidth of 2 MHz was used to pass signals around the operation frequency and filter out signals at the remaining frequency region. The number of elements that can be used in the calculation has been limited to 32 as in the simulations.

If the example where plane B-scans have been used to detect the slots at an angle of 0° is considered, an offline post processing technique that utilises the full set of measurements from all combinations of transmit and receive has been utilised. This technique is referred to as full matrix capture (FMC) [13]. FMC data has been measured at different axial locations along the aluminium plate. These FMC data have been used in post processing to calculate the plane B-scan response at different frequencies and for different aperture sizes. These different measurements were then compared and the specifications that produce the plane B-scan with maximum image magnitude was considered as optimum. The same measurements have been repeated to identify the optimum design for plane B-scan and the TFM for all the slots at the different orientation angles.

Fig. 9 compares the optimised signal amplitude from simulations and experiments using plane B-scan and TFM. In both cases, the signal has been normalised to the maximum of that at 0°. The figure also shows the optimum design parameters (frequency and array size) for all the different experimental crack orientations. The figure suggests good agreement between experiments and simulations with regard to the signal amplitude and design parameters for both imaging methods (i.e. plane B-scan and TFM).

In the above optimisation problem, it should be noted that the simulated crack with the largest orientation angle (θ_s) will produce the largest specular reflection misalignment with respect to the array response function and hence will have the minimum signal amplitude. As a result, the optimisation of the objective function given by equation (6) will always tend to maximise the signal of the crack with the largest orientation angle.

It is also worth mentioning that for a normal distribution, three times the standard deviation for a zero-mean normal distribution accounts for 99.7% of the whole population. For example, a population of cracks with 0° mean and 4° standard deviation PDF will have 99.7% of its samples between -12° and +12°. Therefore, in order to compare experiments to simulations, the optimum parameters calculated experimentally for each crack are assumed to be the same optimum parameters for cracks with orientations that have a zero-mean normally distributed PDF and a standard deviation equivalent to a third of the angle of the experimental crack. Therefore, the optimum calculation for samples with 0, 15, 30, 45° cracks are approximated by the optimum calculations for samples that have cracks with zero-mean normally distributed PDFs and standard deviations (σ_s) of 0, 5, 10, 15°, respectively.

3.2. Example 2: optimising frequency, pitch size, total and aperture sizes

In this more realistic, multi-parameter example, a 1-D array with the specifications shown in Table 3 is used. Here, it is assumed that the defective region is known and so the array is located such that it is always aligned with the location of the crack. It is also assumed that the array size is limited, perhaps due to access constraints.

Fig. 6 (b) shows a schematic diagram that describes this inspection set up.

In this case the size of the array (N), aperture size (N_A), element pitch (p), and the operational angular frequency (ω) are considered as the optimisation variables.

The objective function in this example has been chosen to be the array signal to noise ratio of the worst-case-scenario (i.e. the response from the crack that produces the minimum signal to noise ratio). The signal to noise ratio in this case is assumed to be the ratio between the signal amplitude from the defect (calculated using the forward model of equation 1 and equation 2 or 3 depending on the imaging algorithm used) to the RMS noise value (calculated using equation 4). Mathematically, the optimisation problem can be expressed using this objective function as follows:

$$\max snr(\pmb{e}', N, N_A, p, \omega)_{min} \tag{7}$$

where

$$snr_{min}(\pmb{e}', N, N_A, p, \omega) = \left(\frac{I(\pmb{e}', N, N_A, p, \omega)}{\sqrt{\langle|n(\pmb{e}, N, N_A, p, \omega)|^2\rangle}}\right)_{min} \tag{8}$$

and the values of N, N_A, p, and ω are constraints by the values shown in Table 3.

It has to be noted that for plane B-scan imaging, the element pitch and width are largely irrelevant. Therefore, minimum pitch and width sizes have been chosen.

3.2.1. Optimisation results

Results for the optimum design parameters using the plane B-scan and the TFM are shown in Table 4.

3.3. Discussion

In example 1, and if we consider the case when there is only one crack with a 0° orientation angle (i.e. $\theta_s = 0°$ and $\sigma_s = 0°$), Table 2 and Fig. 9 suggest that, for the plane B-scan algorithm, the optimum frequency is 7 MHz, which is the maximum allowed frequency. In this case, it is possible for the array to measure the specular reflection from the crack and in order to maximise the response the frequency is increased. However, as the orientation angle standard deviation increases, this alignment between the beam profile and the defect scattering coefficient does not remain. Therefore, the optimal array frequency decreases and the size of the optimal aperture increases to achieve wider beam width and hence receive more energy. Increasing the aperture size will also increase the amount of noise in measurements. As this example is optimising signal amplitude only, noise does not affect result.

The same principles apply for the TFM. The only difference is that because of its focusing abilities, maximum frequency has always been achieved as an optimum value for all the different standard deviations that have been explored in this study. The only limiting factor for achieving maximum frequency in the case of TFM is the individual array element directivity. It is expected that beyond a certain σ_s, the optimal frequency would decrease to achieve higher signal amplitude. A maximum aperture is always the optimum in TFM imaging case because delay laws applied ensure that all the signals are superimposed constructively.

Optimising the signal-to-noise ratio, as has been done in example 2, produces different design parameters for plane B-scan imaging. It can be noted that as the orientation angle standard deviation increases, the optimal frequency initially tends to increase towards the maximum allowable value and the aperture size tends to decrease to achieve maximum signal-to-noise ratio. Additionally, the array size increases as the orientation

increases indicating the system's attempt to always capture the specular reflections from the different defects.

When TFM is used, maximum frequency and maximum aperture size have always been observed as optimum for all values of crack orientations. It can be noted that a pitch size of 0.36 mm ($\approx \lambda/2$) has come out as optimum pitch size for all investigated crack orientations. It is interesting to note that linear arrays are often currently designed with a pitch size of $\lambda/2$ to entirely eliminate the effect of noise and artefacts associated with grating lobes. Similarly, in the optimisation scheme, one of the main factors that governs the pitch size is that grating lobe noise increases as the pitch size increases which adversely affects the signal to noise objective function.

The optimum design parameters from and Table 4 can be used to assess the performance of the array and calculate the ROC curves as shown in Fig. 10. the probability of detection (P_D) has been calculated from the different values of the signal amplitude from the defects using equation 1, while the probability of false alarm (P_{FA}) has been calculated assuming that the noise can be described as zero-mean normally distributed random signal with a standard deviation that can be calculated using equation 4. It can be noted from these ROC curves that the TFM achieves higher P_D than that achieved by the plane B-scan at all cases with lower P_{FA}.

4. Conclusions

A general framework for the optimisation of ultrasonic array inspection techniques in NDE has been presented. Inspection uncertainty has been incorporated by employing a deterministic forward model and then a Monte Carlo approach is used to heuristically simulate the stochastic nature of the inspection. The main focus was on defect detection hence a binary hypothesis test was adopted, and receiver operating characteristic (ROC) curves were used to characterise the performance.

This system has been used in two simple examples to optimise array measurements of cracks in aluminium plates. 3 mm cracks were assumed to exist in the aluminium plates at a depth of 20 mm. The crack orientation angle is assumed to be random with a normally distributed PDF, $N(\mu_s, \sigma_s)$. Its mean (μ_s) is always assumed to be 0 while different crack orientation standard deviations (σ_s) have been used throughout the simulations (0, 2, 4, 6, 8, 10 and 15°). The capabilities of this optimisation system have been demonstrated by exploring objective functions based on the array signal amplitude and signal to noise ratio for plane B-scan and TFM imaging. Many design parameters have been investigated such as the size of the array, size of array aperture, frequency, and element and pitch sizes.

The simulations in this paper demonstrate the robustness and versatility of TFM compared to plane B-scan. The same TFM inspection design (maximum frequency and array size) was fond to be optimal for the detection of defects using the amplitude and

signal-to-noise based objective functions and a number of statistical distributions of crack orientation angles.

The intention in this study is to demonstrate a general framework design that can be used to examine different inspection scenarios, uncertain parameters, imaging algorithms, and objective functions. In this paper, crack orientation was the only uncertainty considered in the demonstration examples. However, defect type, size, and location and material geometry and properties can easily be considered. More design parameters can be dealt with as well. It is expected that the computational requirements of the system will increase as the number of uncertain parameters and optimisation variables increase. Parallel computing and GPU capabilities could be utilised to further speed up the optimisation process.

5. References

[1] Mahaut S, Roy O, Beroni C, Rotter B. Development of phased array techniques to improve characterization of defect located in a component of complex geometry. Ultrasonics. 2002;40:165-9.

[2] Matte GM, Van Neer PLMJ, Danilouchkine MG, Huijssen J, Verweij MD, de Jong N. Optimization of a Phased-Array Transducer for Multiple Harmonic Imaging in Medical Applications: Frequency and Topology. IEEE Trans. Ultrason. Ferr. Freq. Cont. 2011;58:533-46.

[3] Ergun AS. Analytical and numerical calculations of optimum design frequency for focused ultrasound therapy and acoustic radiation force. Ultrasonics. 2011;51:786-94.

[4] Nikolov M, Behar V. Simulated annealing optimization of multi-element synthetic aperture imaging systems. Lect. Notes Comput. Sc. 2008;4818:585-92.

[5] Martinez-Graullera O, Martin CJ, Godoy G, Ullate LG. 2D array design based on Fermat spiral for ultrasound imaging. Ultrasonics. 2010;50:280-9.

[6] Raju BI, Hall CS, Seip R. Ultrasound Therapy Transducers With Space-Filling Non-Periodic Arrays. IEEE Trans. Ultrason. Ferr. Freq. Cont. 2011;58:944-54.

[7] Mahaut S, Darmon M, Chatillon S, Jenson F, Calmon P. Recent advances and current trends of ultrasonic modelling in CIVA. Insight. 2009;51:78-81.

[8] Zhang J, Drinkwater BW, Wilcox PD, Hunter AJ. Defect detection using ultrasonic arrays: The multi-mode total focusing method. NDT&E Int. 2010;43:123-33.

[9] Puel B, Lesselier D, Chatillon S, Calmon P. Optimization of ultrasonic arrays design and setting using a differential evolution. NDT&E Int. 2011;44:797-803.

[10] Flynn EB, Todd MD. A Bayesian approach to optimal sensor placement for structural health monitoring with application to active sensing. Mech. Syst. Signal Pr. 2010;24:891-903.

[11] Schmerr JL. Fundamentals of Ultrasonic Nondestructive Evaluation: A Model Approach. Plenum Press: New York; 1998.

[12] Glushkov E, Glushkova N, Ekhlakov A, Shapar E. An analytically based computer model for surface measurements in ultrasonic crack detection. Wave Motion. 2006;43:458-73.

[13] Holmes C, Drinkwater BW, Wilcox PD. Post-processing of the full matrix of ultrasonic transmit-receive array data for non-destructive evaluation. NDT&E Int. 2005;38:701-11.

[14] Wilcox PD. Array Imaging of Noisy Materials. AIP Conf. Proc. 2011;1335:890-7.

[15] Margetan FJ, Thompson RB, Yalda I. Backscattered Microstructural Noise in Ultrasonic Toneburst Inspections. J. Non-destr. Eval. 1994;13:111-36.

[16] Yalda I, Margetan FJ, Thompson RB. Predicting ultrasonic grain noise in polycrystals: A Monte Carlo model. J. Acoust. Soc. Am. 1996;99:3445-55.

[17] Connolly GD, Lowe MJS, Temple JAG, Rokhlin SI. Correction of ultrasonic array images to improve reflector sizing and location in inhomogeneous materials using a ray-tracing model. J. Acoust. Soc. Am. 2010;127:2802-12.

[18] Mitchell M. An introduction to genetic algorithms. Cambridge, Mass.: MIT Press; 1996.

[19] Kay SM. Fundamentals of statistical signal processing. Englewood Cliffs, N.J.: Prentice-Hall PTR; 1993.

[20] Drinkwater BW, Wilcox PD. Ultrasonic arrays for non-destructive evaluation: A review. NDT&E Int. 2006;39:525-41.

[21] Miller GF, Pursey H. The Field and Radiation Impedance of Mechanical Radiators on the Free Surface of a Semi-Infinite Isotropic Solid. Proc. Roy. Soc. Lond. Ser-A. 1954;223:521-41.

Fig. 1. Flowchart diagram of the proposed optimisation framework.

Fig. 2. Schematic diagram of the generalised forward model.

Fig. 3. Point spread function of a TFM image in aluminium using 32 element 5 MHz 0.63 mm pitch ultrasonic phased array.

Fig. 4. $p(h; H_1)$ and $p(h; H_0)$ are the PDFs of signal (I) and noise (n) for hypothesis testing problem, respectively.

Fig. 5. (a) Schematic diagram of the test structure used for both simulation and experiment. In the case of the simulations, θ_s is random while in the case of experiments, $\theta_s = 0, 15, 30, 45°$. (b) the normally distributed PDF of the crack orientation angle θ_s which is used in simulations.

Fig. 6. (a) Schematic diagram for the inspection set up in example 1. $\omega/2\pi$ and N_A are the optimisation variables, array element pitch is 0.63 mm and mechanical scanning along the aluminium plate indicated by the arrows is used. (b) Schematic diagram for the inspection set up in example 2. $\omega/2\pi$, N_A, N, and p are the optimisation variables. The array is fixed at the location where its centre is directly above the location of the defect.

Fig. 7. Evolution of objective function (signal amplitude, I_{min}) (top) and the decision variables: angular frequency, $\omega/2\pi$ (middle) and aperture size, N_A (bottom) using plane B-scan (left) and TFM (right).

Fig. 8. Imaging of the 0° 3mm crack (as in schematic diagram (a)) using (c) plane B-scan with 7 MHz frequency and 7.6 mm size array, (e) plane B-scan with 3 MHz frequency and 18.3 mm size array, (i) TFM with 7 MHz frequency and 20.2 mm size array. Imaging of the 45° 3mm crack (shown in schematic diagram (b)) using (d) plane B-scan with 7 MHz frequency and 7.6 mm size array, (f) plane B-scan with 3 MHz frequency and 18.3 mm size array, (j) TFM with 7 MHz frequency and 20.2 mm size array. Figures (g) and (h) compare the magnitudes in the axial direction of images (c) and (e) and (d) and (f), respectively.

Fig. 9. Optimised signal amplitudes from simulations and experiments using (a) plane B-scan and (b) TFM.

Fig. 10. ROC curves for the optimum design to detect cracks with 0, 2, 4, 6, 8, 10, and 15° STD using snr_{min} as objective function and plane B-scan and TFM.

Table 1. Array transducer parameters used in example 1.

Table 2. Array size (N_A) and angular frequency (ω) for optimum design using the objective function $I_{min}(\boldsymbol{e'}, N_A, \omega)$ for the different crack orientation standard deviations, σ_s.

Table 3. Array transducer parameters used in example 2.

Table 4. Optimum design parameters for the objective function $snr_{min}(\boldsymbol{e'}, N, N_A, p, \omega)$ for the different crack orientation standard deviations.

Fig1

Fig2

Fig3

Fig4

Fig5

Fig6

(a)

$\omega/2\pi$ N_A

0.63 mm

(b)

$\omega/2\pi$ N

N_A

p

Fig7

Fig8

(a)

20 mm

(b)

20 mm   45°

(c)

(d)

(e)

(f)

(g)
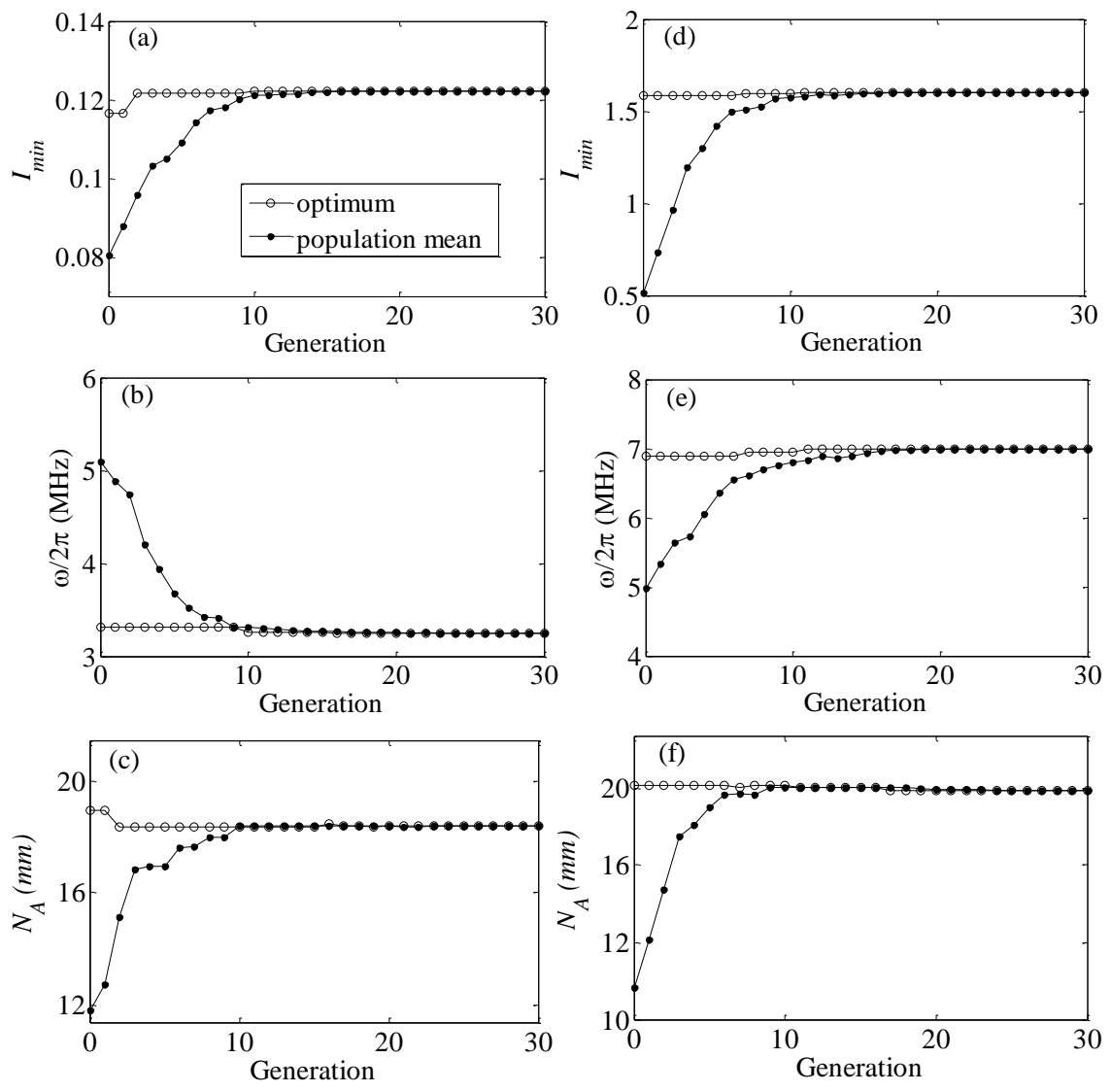

7MHz, 7.6mm
3 MHz, 18.3 mm

(h)

(i)

(j)
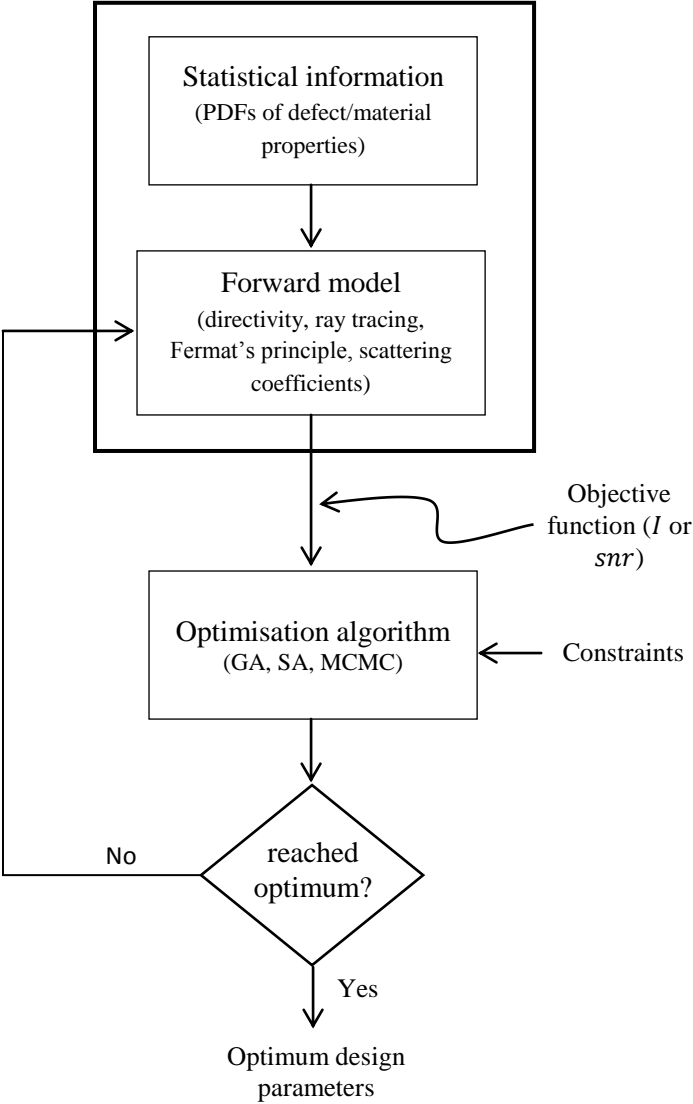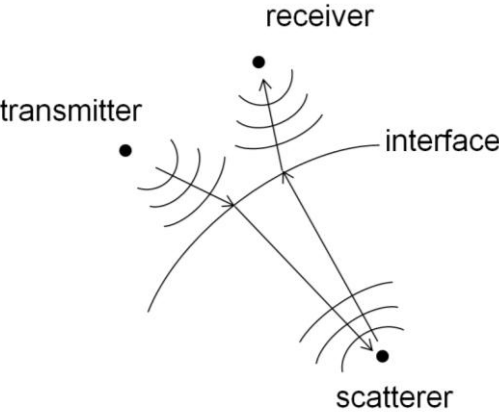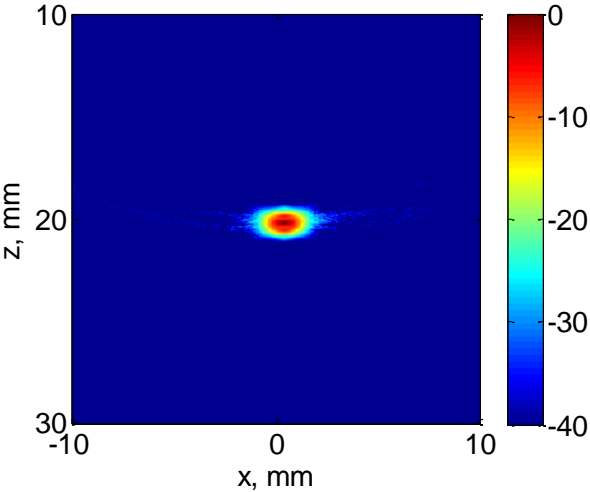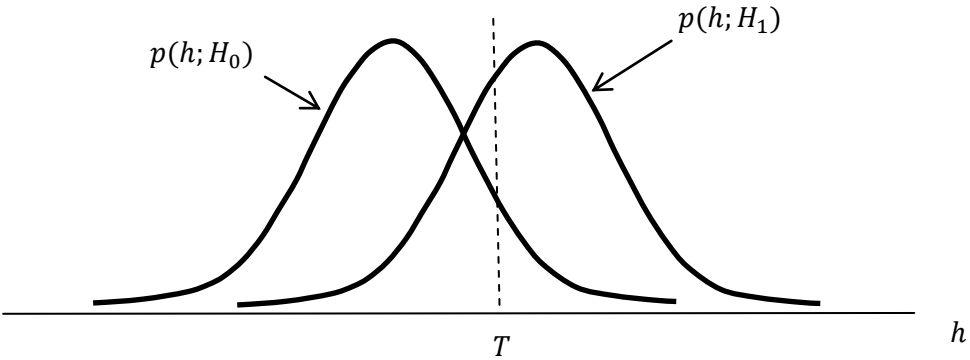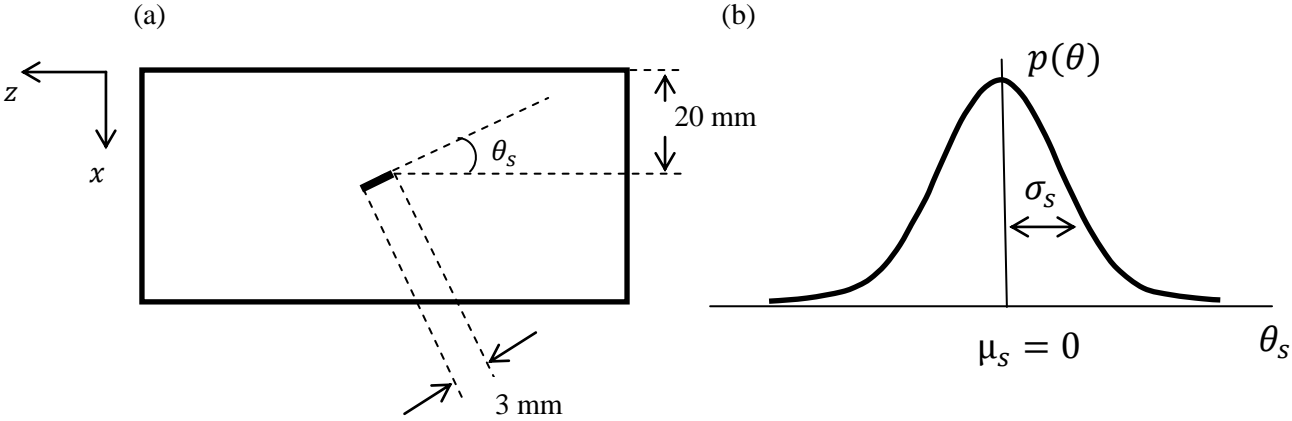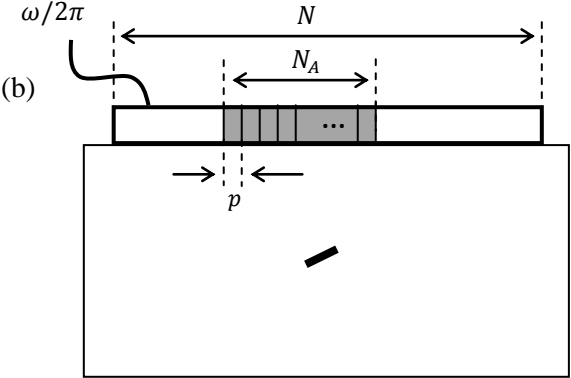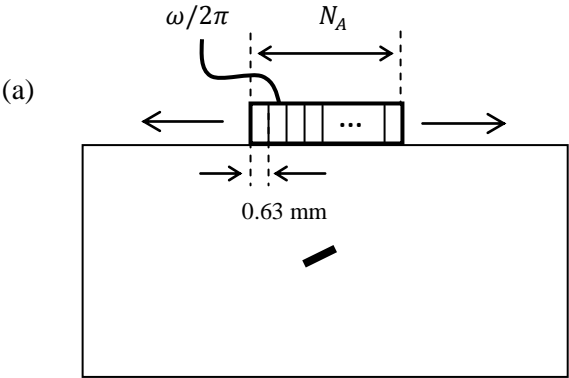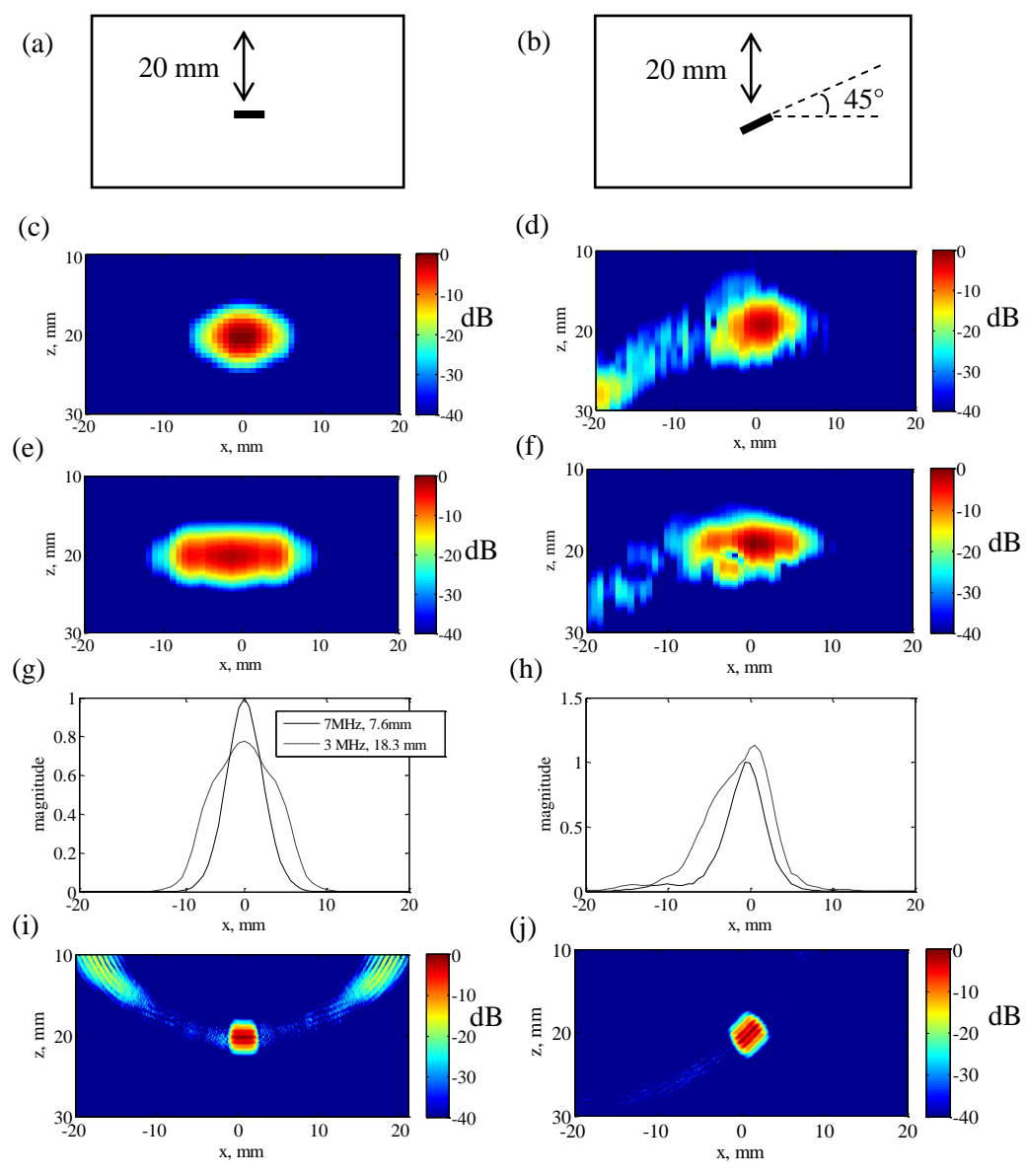
Fig9
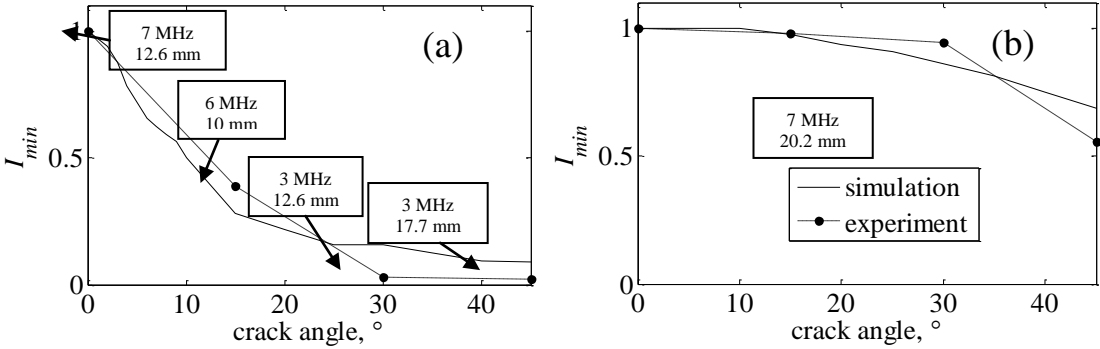
Fig10
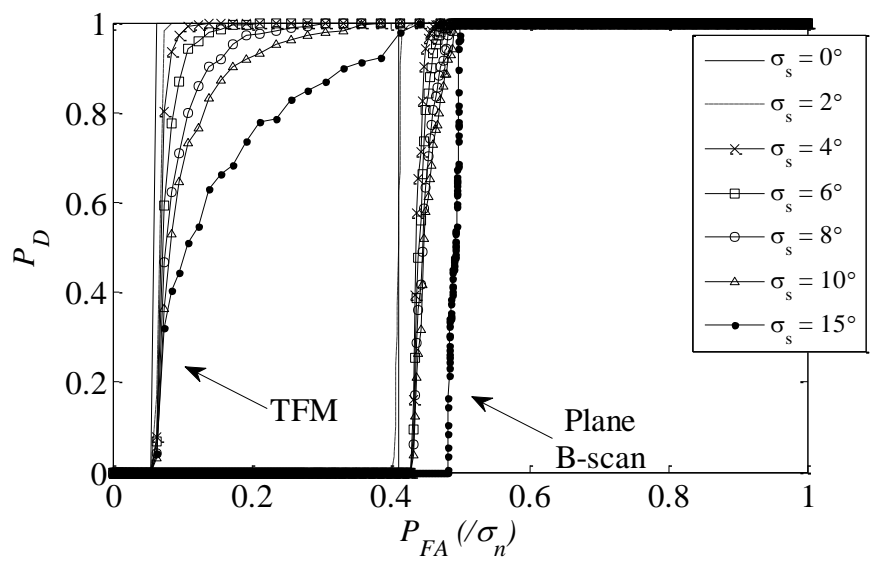
Table 1. Array transducer parameters used in example 1.

Array parameter	Value
Aperture size, N_A (mm)	0.63-20.2
Element pitch, p (mm)	0.63
Element width, a (mm)	0.53
Frequency, $\omega/2\pi$ (MHz)	3-7

Table 2. Array size (N_A) and angular frequency (ω) for optimum design using the objective function $I_{min}(e', N_A, \omega)$ for the different crack orientation standard deviations, σ_s.

Plane B-scan

σ_s (°)	Frequency, $\omega/2\pi$ (MHz)	Aperture size, N_A (mm)
0	7	7.6
2	4.5	9.5
4	3.2	18.3
6	3.2	18.3
8	3	18.3
10	3	18.3
15	3	18.3

TFM

σ_s (°)	Frequency, $\omega/2\pi$ (MHz)	Aperture size, N_A (mm)
0,2,4,6,8,10, and 15	7	20.2

Table 3. Array transducer parameters used in example 2.

Array parameter	Value
Array size, N (mm)	0.315-20.2
Aperture size, N_A (mm)	0.315-20.2
Element pitch, p (mm)	0.315-6.3
Element width, a (mm)	($p-0.1$)
Frequency, $\omega/2\pi$ (MHz)	1-10

Table 4. Optimum design parameters for the objective function $snr_{min}(\boldsymbol{e'}, N, N_A, p, \omega)$ for the different crack orientation standard deviations.

Plane B-scan

σ_s (°)	Frequency, $\omega/2\pi$ (MHz)	Aperture size, N_A (mm)	Array size, N (mm)
0	7.7	8.8	10
2	7.5	8.6	11
4	10	1.3	13
6	10	1.3	16
8	10	1.3	20
10	10	1.3	20
15	7.6	10	13

TFM

σ_s (°)	Frequency, $\omega/2\pi$ (MHz)	Element pitch, p (mm)	Aperture size, N_A (mm)	Array size, N (mm)
0,2,4,6,8,10, and 15	10	0.36	20.2	20.2